Phase behavior and collective excitations of the Morse ring chain

A. Chetverikov and J. Dunkel[2,a]

[1] Faculty of Nonlinear Processes, Saratov State University, Astrakhanskaya 83, 410012 Saratov, Russia
[2] Institute of Physics, Humboldt-Universität zu Berlin, Newtonstrasse 15, 12489 Berlin, Germany

Abstract. Using primarily numerical methods we study clustering processes and collective excitations in a one-dimensional ring chain. The ring chain is constituted by N identical point particles with next neighbors interacting via nonlinear Morse springs. If the system is coupled to a heat bath (Gaussian white noise and viscous friction), then depending on the particle density and the bath temperature different phase-like states can be distinguished. This will be illustrated by means of numerically calculated phase diagrams. In order to identify collective excitations activated by the heat bath we calculate the spectrum of the normalized dynamical structure factor (SDF). Our numerical results show that the transition regions between different phase-like states are typically characterized by a $1/f$-type SDF spectrum, reflecting the fact that near critical points correlations on all length and time scales become important. In the last part of the paper we also discuss a non-equilibrium effect, which occurs if an additional nonlinearly velocity-dependent force is included in the equations of motions. In particular it will be shown that such additional dissipative effects may stabilize cluster configurations.

PACS. 05.70.Fh Phase transitions: general studies – 05.70.Ln Non-equilibrium and irreversible processes – 05.40.-a Fluctuation phenomena, random processes, noise and Brownian motion

1 Introduction

Initiated by the pioneering work of Fermi, Pasta and Ulam [1], studies of nonlinear one-dimensional model systems have essentially contributed to the understanding of nonlinear effects in physical systems, such as polymers and quasi-1D-lattices [2]. Fundamental analytic results in this field of research were obtained by Toda [3,4] in the early 1980's, when he was able to find exact solutions for the dynamics and statistical thermodynamics of a chain with exponentially repulsive next neighbor (n.n.) interactions. In particular, Toda calculated the exact partition function of this model and proved the existence of soliton excitations for the case of an infinite chain. Nonlinear soliton-like excitations propagating in finite Toda chains with periodic boundary conditions are referred to as cnoidal waves. The coupling of finite size Toda ring chains to a heat bath (white noise) and properties of the resulting excitation spectra are, for instance, discussed in [5–8].

Recently, the investigation of cnoidal waves was extended to systems featuring nonlinear dissipation, both on the theoretical [9,10] as well as on the experimental sector [11]. In this context, the concepts of negative friction and active Brownian motion play an important role [12–14]. Moreover, also several types of more complicated nonlinear n.n. interactions were analyzed, *e.g.*,

interactions based on Lennard-Jones and Morse potentials [15–18]. These models exhibit several new phenomena, *e.g.*, clustering effects, since in contrast to the effectively purely repulsive forces in Toda ring chains the respective potentials can also lead to attraction, if the distance between n.n. becomes sufficiently large.

In the present paper we continue the numerical investigation of thermal excitations and clustering processes in one-dimensional Morse ring chains with small particle number N [16,17]. In particular, phase diagrams for the case $N = 4$ are determined. In order to analyze collective excitations in presence of a Gaussian heat bath, we use the dynamical structure factor (SDF) [19]. This quantity has already been successfully applied in previous theoretical investigations of finite-size ring chains with Toda and Lennard-Jones interactions [20,21]. Another important reason for studying the SDF is that it can be measured directly for real systems in inelastic scattering experiments. With regard to the results we can anticipate, that a strong correlation between $1/f$-behavior in SDF spectrum and phase transition-like events in the chain is found.

The paper is organized as follows. In Sections 1.1 and 1.2 we introduce the equations of motion and review essential results from earlier investigations. Section 2 gives a survey of the numerical algorithms and of the quantities, typically measured in the simulations (cluster distributions, structure factor etc.). In Section 3 results for

[a] e-mail: dunkel@physik.hu-berlin.de

the equilibrium system with purely linear friction are presented, and in Section 4 we begin the discussion of nonequilibrium effects. Finally, Section 5 contains a summary of the main results.

1.1 Equations of motion

We consider a one-dimensional model of N identical Brownian point-particles with masses m. Each particle is described by its position coordinate $x_i(t)$ and velocity $v_i(t)$, $i = 1, \ldots, N$. Throughout this paper, we assume periodic boundary conditions

$$x_{i+N} = x_i + L, \tag{1}$$

that is, we consider a ring of length L. For our model the full potential energy stored in the ring reads

$$U = \sum_{i=1}^{N} U_i^M(r_i), \tag{2}$$

where $U_i^M(r_i) = U_i^M(x_{i+1} - x_i)$ denotes the Morse pair interaction potential [15] explicitly given by

$$U_i^M(r_i) = \frac{a}{2b} \left[e^{-b(r_i - \sigma)} - 1 \right]^2 - \frac{a}{2b} \tag{3}$$

with positive parameters $a, b, \sigma > 0$. Originally, this potential, which is qualitatively very similar to the well-known Lennard-Jones (LJ) potential

$$U_i^{LJ}(r_i) = \frac{a}{2b} \left[\left(\frac{r_i}{\sigma} \right)^{-12} - 2 \left(\frac{r_i}{\sigma} \right)^{-6} \right], \tag{4}$$

was used to describe diatomic molecules. Inserted into Schrödinger's equation the Morse potential allows the exact calculation of the vibrational energy levels [15]. As evident from (3) and (4), and also illustrated in Figure 1a, both Morse and LJ potential take their only minimum at $r_i = \sigma$ and tend asymptotically to 0 for $r_i \to \infty$. Accordingly, their depth ε is defined by

$$\varepsilon := U_i^{M/LJ}(\infty) - U_i^{M/LJ}(\sigma) = \frac{a}{2b}. \tag{5}$$

The Morse potential (3) can also be considered as a generalization of Toda's exponential potential [3]

$$U_i^T(r_i) = \frac{a}{b} \left[e^{-b(r_i - \sigma)} - 1 \right] + a(r_i - \sigma) - \frac{a}{2b}, \tag{6}$$

widely appreciated due to the fact, that it yields an exactly solvable nonlinear model. In (3) and (6) the parameter a controls the amplitude of the corresponding force, whereas b can be interpreted as the stiffness parameter of the spring that connects two interacting particles. In this picture σ gives the equilibrium length of such a spring. For all three potentials the angular frequency ω_0 near the minimum is defined as

$$\omega_0 = \frac{1}{m} \sqrt{\frac{d^2 U_i}{dr^2}(\sigma)}, \tag{7}$$
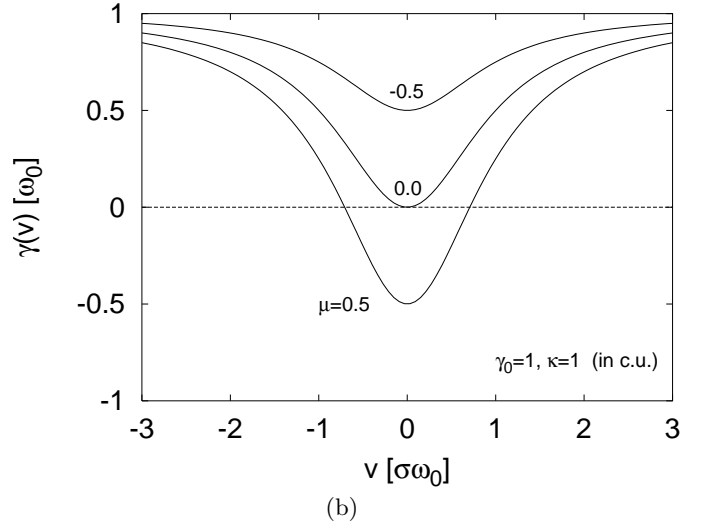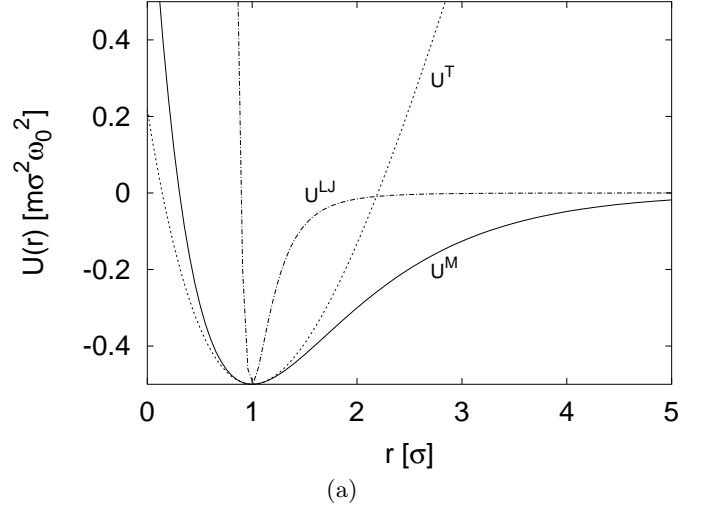
Fig. 1. (a) Morse potential $U^M(r)$, LJ potential $U^{LJ}(r)$ and Toda potential $U^T(r)$ for the parameter value $b = 1$. For $r \ll \sigma$ a Morse force with parameter b behaves like a Toda force with parameter $2b$. (b) Friction coefficient $\gamma(v) = \gamma_0 + \gamma_1(v)$ for different parameter values μ. In case of $\mu < 0$ the friction coefficient is always positive (pure damping), whereas for $\mu > 0$ there also exists a negative (pumping) region. For high absolute velocities $v^2 \gg \mu$ we observe that $\gamma(v) \to \gamma_0$ holds, *i.e.*, in this limit the dynamics reduces to standard Brownian motion. Remark on the units: In the characteristic unit system (*c.u.*) defined by $m = \omega_0 = \sigma = 1$ we obtain $[a] = m\sigma\omega_0^2$, $[b] = \sigma^{-1}$, $[r] = \sigma$, $[U] = m\sigma^2\omega_0^2$, $[\gamma(v)] = \omega_0$, $[v] = \sigma\omega_0$, $[\mu] = [\kappa] = \sigma^2\omega_0^2$.

and one finds explicitly

$$\omega_0 = \omega_0^{M/T} = \frac{\omega_0^{LJ}}{3\sqrt{8}} = \sqrt{\frac{ab}{m}}. \tag{8}$$

One may further notice, that the linear (attractive) part of the Toda potential (6) has *no effect* on the dynamics, if a ring chain is considered. This fact follows directly, if one

inserts the Toda potential into the Langevin equations

$$\frac{d}{dt}x_i = v_i,$$

$$m\frac{d}{dt}v_i + \frac{\partial U}{\partial x_i} = -m\,\gamma(v_i)\,v_i + \sqrt{2D}\,\xi_i(t), \qquad (9)$$

governing the stochastic motion of the ith particle on the ring. The stochastic forces $\sqrt{2D}\,\xi_i(t)$, which model a surrounding heat bath (Gaussian white noise), are characterized by

$$\langle \xi_i(t) \rangle = 0, \qquad \langle \xi_i(t')\xi_j(t) \rangle = \delta_{ij}\,\delta(t'-t). \qquad (10)$$

In the present paper we confine ourselves to cases where the velocity-dependent friction coefficient can be written in the form

$$\gamma(v) = \gamma_0 + \gamma_1(v). \qquad (11)$$

Here only the constant part γ_0 describes the viscous friction between particle and surrounding heat bath. In fact, the biggest part of this paper is dedicated to the standard equilibrium situation where $\gamma_1(v) \equiv 0$. Only in the last part we are going to consider the following additional nonlinear coefficient

$$\gamma_1(v) = -\frac{q}{(c/d_2) + v^2}. \qquad (12)$$

This friction coefficient was introduced in [14,22,23] to model active Brownian particles that carry refillable energy depots (internal degrees of freedom). In (12) the parameter $q > 0$ describes the flux of energy from an external reservoir or field into the depots carried by the particles. The parameter $c > 0$ is connected to internal dissipation and $d_2 > 0$ controls the conversion of the energy taken up from the external field into kinetic energy. Actually, the parameter q and the ratio

$$\kappa = c/d_2 \qquad (13)$$

are the essential parameters of this model. The parameter choice $\kappa = 0$, for example, describes particles without internal dissipation. In the limit cases $q = 0$ and $\kappa = \infty$ (no energy conversion) we regain the equilibrium system, characterized by purely viscous friction, $\gamma(v) \equiv \gamma_0$.

If one is interested in the non-equilibrium case, $\gamma_1(v) \neq 0$, then it is convenient to introduce a new parameter

$$\mu = \frac{q}{\gamma_0} - \kappa, \qquad (14)$$

and to rewrite

$$\gamma(v) = \gamma_0 \left(1 - \frac{\kappa + \mu}{\kappa + v^2}\right) = \gamma_0 \,\frac{v^2 - \mu}{\kappa + v^2}. \qquad (15)$$

Obviously the parameter μ plays the role of a bifurcation parameter since $\gamma(v) = 0$ if $v = \pm\sqrt{\mu}$. In terms of μ one can summarize the effect of the combined friction coefficient $\gamma(v)$ as follows:

(i) For $\mu < 0$ the friction coefficient $\gamma(v)$ is always positive, and therefore leads to damping of the particle motion;

(ii) according to (15) for $\mu > 0$ the effective friction coefficient $\gamma(v)$ converges to γ_0 for large velocities $v^2 \gg \mu$, but for small velocities $v^2 < \mu$ the friction coefficient $\gamma(v)$ is negative, generating so-called active motions.

Conventionally, we shall speak of active Brownian particles if $q > 0$ holds. In Figure 1b we have plotted the friction coefficient $\gamma(v)$ for different values of μ.

Characteristic units

In order to reduce the number of parameters in our model it is useful to choose an appropriate set of characteristic units ($c.u.$) Since we intend to focus on homogeneous rings, a natural choice corresponds to the unit system where $m = 1$, $\sigma = 1$ and $\omega_0 = 1$ holds. Obviously, the first two conventions simply correspond to fixing unit mass and unit distance, whereas the third gives a characteristic unit time, because ω_0 was defined as the angular frequency for the Morse potential. Choosing these $c.u.$, our working equations take the form

$$\frac{d}{dt}x_i = v_i,$$

$$\frac{d}{dt}v_i + \frac{\partial U}{\partial x_i} = \gamma_0 \left[\frac{\kappa + \mu}{\kappa + v_i^2} - 1\right]v_i + \sqrt{2D}\,\xi_i(t). \qquad (16)$$

In particular, for the parameters a and b of the Morse potential we find that $a = 1/b$ in $c.u.$ Conventionally, from now on all quantities appearing in equations, diagrams etc. will be given in $c.u.$

Fluctuation-dissipation-theorem

We conclude this part with a remark on the fluctuation-dissipation theorem (FDT). Generally, the FDT links the amplitude D of the stochastic force with the physical temperature T of the heat bath and the *viscous* friction coefficient $\gamma(v)$. Now it is important to notice, that we assume in our model, that the nonlinear part $\gamma_1(v)$ is absolutely independent of the fluctuations in the heat bath. Occupying this point of view, it is reasonable to postulate that the Einstein relation, which reads for $k_B = 1$

$$D = T\gamma_0\,, \qquad \text{(in } c.u.), \qquad (17)$$

is also valid for our non-equilibrium system [16]. Hence, whenever we speak of the temperature T below, we exclusively refer to the temperature of the heat bath. We emphasize that, in general, T will be non-trivially connected with the average kinetic energy T_{kin} of active particles.

An extensive discussion of examples, where the FDT differs from the Einstein relation (17), as for instance in models with velocity-dependent *viscous* friction coefficients, can be found in [24].

1.2 Some results of previous studies

We already anticipated above that, compared with Toda rings, in Morse ring chains new phenomena such as clustering may arise. The main reason for this is that, in contrast to the effectively purely repulsive Toda interaction, the Morse potentials lead to attractive forces between n.n., if their distance is sufficiently large. This observation implies that the mean particle density

$$n := N/L \tag{18}$$

is one of the most important macroscopic quantities for the characterization of Morse rings. Of course, the same is true for the qualitatively very similar Lennard-Jones interactions.

In order to illustrate the effects of a density variation, it is convenient to consider the related change of the full potential energy

$$U^{T/M}(x_1, \ldots, x_N) = \sum_{i=1}^{N} U_i^{T/M}.$$

We say that a particle configuration is a *stable state* of the ring, if it realizes a local minimum of $U^{T/M}$. Due to the purely repulsive interaction in the Toda case it is clear that for arbitrary values of n there is only one stable state given by the equidistant configuration (more precisely, this minimum of U^T is degenerated with respect to rotations of the ring, but this is not relevant for our discussion). In contrast to the n-invariant structural behavior of U^T, one can show that in Morse rings depending on the density n there may exist different types of stable states [17]. In particular, it can be proved that for an arbitrary particle number N the equidistant configuration corresponds to a minimum of U^M only as long as

$$n > \frac{b}{\ln 2 + b} =: n_c \tag{19}$$

Otherwise, the equidistant configuration becomes a maximum of U^M and, therefore, unstable. Thus, in the *high density* limit $n \gg n_c$ Morse and Toda rings are qualitatively similar. In particular, one can show that for $n \to \infty$ Morse rings with parameter b behave like Toda rings with parameter $2b$. Intuitively, this becomes clear if one considers the square in definition of the Morse potential, see equation (3).

However, for Morse rings there still exists a *second critical* value $\bar{n}_c(N) \geq n_c$, such that for $n < \bar{n}_c(N)$ new minima of U^M can be observed. These new stable states can be identified as N equivalent configurations each corresponding to a single cluster of size N, see rightmost configuration in Figure 2, which we refer to as 'N-mer' in the following. Only for the simplest nontrivial case of a ring with $N = 2$ particles the two critical density values are equal, $n_c = \bar{n}_c(2)$, and for $N = 3$ one finds

$$\bar{n}_c(3) = \frac{3b}{\ln \frac{27}{4} + 3b} > n_c. \tag{20}$$

(1, 1, 1) (1, 1, 0) (1, 0, 0)
           (1, 0, 1) (0, 1, 0)
           (0, 1, 1) (0, 0, 1)
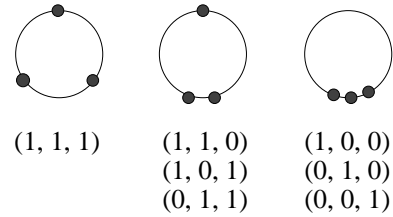
Fig. 2. Schematic representation of the Morse ring with $N = 3$ particles. The vectors (s_1, s_2, s_3) indicate, whether the particle i is the first particle of a cluster (then $s_i = 1$) or not ($s_i = 0$). This labeling of configurations yields a simple counting procedure for the number of critical points of U^M. The equidistant configuration $(1, 1, 1)$ is a minimum of U^M as long as the density is high, $n > n_c$. The three cluster configurations (right) correspond to minima of U^M if the density is low, $n < \bar{n}_c(3)$. In the critical interval $(n, \bar{n}_c)$ both equidistant and cluster configurations are stable states. Finally, configurations in the middle represent saddle-points of U^M if $n < \bar{n}_c(3)$.

Furthermore, numerical calculations have shown that $\bar{n}_c(N)$ increases monotonically with N, even though it is in principle bounded from above by $n = 1/\sigma$. The main consequence of these results is that there exists a transition interval $(n_c, \bar{n}_c)$ for $N \geq 3$, where *both* the N-mers and the equidistant configuration represent stable states; put differently, there is a coexistence region for qualitatively very different stable states.

In the remaining *low density* region $n < n_c$ the N-mers are the only stable configurations, and one can evaluate $Z_N^s = 2^N - 2 - N$ as lower boundary for the number of saddle points in the $(N-1)$-dimensional potential energy landscape U^M. These metastable points correspond to symmetric combinations of smaller clusters ('k-mers' with $1 \leq k < N$), as illustrated for $N = 3$ in Figure 2.

Before we proceed by discussing some of the numerical methods applied in the investigations, it might be useful to summarize the main features of the model once again in brief:

(i) In the high density limit Morse ring chains with parameter b behave like Toda rings chains with parameter $2b$;

(ii) clustering effects can only occur at sufficiently low density;

(iii) there exists a critical density interval, where both equidistant and cluster configurations correspond to local minima of the potential energy;

(iv) by varying the parameters in the friction coefficient $\gamma_1(v)$ the model can be driven from the thermodynamic equilibrium to far-from-equilibrium states.

In previous studies [16,17] we primarily concentrated on the limit case of high density (Toda limit), $n \gg \bar{n}_c > n_c$, and very low densities, $n \ll n_c$, respectively. Hence, it is also a main objective of this paper to extend the investigation to the critical transition region $(n, \bar{n}_c)$. As we shall see below, the dynamic structure factor (SDF) exhibits a characteristic $1/f$-behavior in this region.

2 Numerical aspects and measured quantities

In contrast to earlier investigations of deterministic systems [10,11,17], which also included extensive analytic discussions, the present paper focuses on numerical results. In this part we give a brief survey of the algorithms used in our studies, and also introduce typical quantities (cluster probabilities, structure factor etc.) measured in the computer experiments.

2.1 Algorithm

The numerical integration of the stochastic Langevin equation (16) was performed by using a fourth-order Runge-Kutta algorithm, especially adapted for solving stochastic problems [25]. We used this special algorithm instead of the more common Euler algorithm, because it yields better results in simulations of dissipative systems with coupling to a heat bath as well as in simulations of the related conservative (deterministic) system, required for the calculation of the dynamic structure factor, which is explained in more detail in Section 2.4.

In all computer experiments the heat bath is realized by Gaussian random numbers taken from a standard normal distribution. Moreover, we always start with equal distances between the particles, $r_i = 1/n$, and all particles initially at rest, $v_i(0) = 0$. The integration step is always fixed as $dt = 0.001$ (in c.u.).

Each simulation consists of two stages: First the ring chain is heated to the given temperature $T = D/\gamma_0$; at the second stationary stage, i.e., when the time averages of characteristic physical quantities do not change anymore, measurements are made. In addition to typical physical quantities as kinetic energy T_{kin}, potential energy U, full energy E or trajectories, we also considered the probability of cluster configurations, the average absolute force and the dynamic structure factor (SDF).

2.2 The probability of cluster configurations

In agreement with [17] we introduce the cluster size variable K, which can take values $k \in \{1, \ldots, N\}$ for a ring with N particles. Then $P_D[K = k]$ is defined as the (stationary) probability for finding a cluster of size k on the ring at time $t \gg 0$, where D is the respective noise strength. For example, in the deterministic limit case $D = 0$ with purely viscous damping $\gamma(v) \equiv \gamma_0$

$$P_0[K < N] = 0, \qquad P_0[K = N] = 1 \qquad (21)$$

if $n < n_c$, since then only the N-mer configurations are stable states. For $D > 0$ the probabilities $P_D[k] = P_D[K = k]$ can only be determined numerically. In computer experiments one can calculate $P_{D>0}[k]$ from the relative frequency of finding a cluster of size k during several independent measurements over time intervals $\Delta t = t_2 - t_1$, where $t_2 > t_1 \gg 0$.

We now still need to define 'clusters'. At low densities $n < n_c$, we define that n.n. particles belong to the same cluster or k-mer, respectively, if their distance r_i is smaller than $1/n_c$. For instance, if $b = 1$ as used in most simulations, then $1/n_c \approx 1.7$ in c.u. Obviously, this definition is in agreement with (21), but also it only makes sense for $n < n_c$. Hence, for the complementary case $n \geq n_c$ we define that a 'cluster state' is observable, if there is at least one r_i with $r_i > 1/n_c$. Otherwise, we speak of a solid-like state. Actually, at supercritical density $n > \max\{n_c, \bar{n}_c\}$ it is more appropriate to say that the chain exhibits *gaps* or strongly *localized compressions*, respectively, if $r_i > 1/n_c$ holds for some r_i.

Note that in this form our 'geometrical' definition of the probabilities $P_D[k]$ does not distinguish between clusters with negative energy $E_{cl} = \sum_i E_i < 0$, where E_i is the sum of kinetic and potential energy of the ith particle in the cluster, and compressions with $E_{cl} > 0$, only existing for a very short time. For example, a nonlinear soliton excited in a dense chain at high temperature may be qualified by this definition as a cluster of constant size, even though the set of particles forming the soliton is permanently changed, while it travels along the chain.

The main reason for us to choose a geometrical definition is that it will work equally well for both equilibrium and non-equilibrium (active) systems. For instance, in an active chain there may also exist very stable clusters, which move at very high velocities on the ring (due to the pumping). This makes it difficult to find a straightforward energetic criterion.

Nevertheless it must be mentioned that especially in a small density region $n \approx n_c$ our criteria are by nature not very trustworthy. In fact, purely geometric definitions are always limited, and to us the use of the characteristic length scale $1/n_c$ seems quite reasonable at this point. It was also checked that moderate variations of the critical distance, $1/n_c \rightarrow 1/n_c \pm \delta$, merely lead to slight quantitative changes in the numerically measured cluster distributions.

2.3 The average force

In addition to the classification of cluster states, we are also interested in thermodynamic properties of finite size rings. Above we already defined the density n and the temperature T in a rather straightforward manner. With regard to the thermodynamic quantity 'pressure' the situation is more complicated, for there is no general rule how to measure pressure for a finite size 1d-system with periodic boundary conditions. Since it is sufficient for our purpose, we are going to consider here the average of the (absolute) forces

$$P := \lim_{\tau \to \infty} \frac{1}{\tau} \int_0^\tau \frac{1}{N} \sum_{i=1}^N \left| \frac{\partial U^M}{\partial x_i} \right| dt, \qquad (22)$$

which is numerically easy to calculate. For simplicity we shall refer to P as pressure, while always keeping in mind the *ad hoc* character of its definition. Below we analyze how P depends on n and T. Then it will turn out that

definition (22) is quite useful. We still remark that (22) does not include static pressure, and that without taking the absolute values the sum in (22) would vanish.

2.4 The dynamic structure factor (SDF)

The dynamic structure factor (SDF) is a useful tool in the analysis of collective excitations [5,6,19–21]. All results presented below are based on the following definition of the SDF [19]

$$S(\omega,k) = \frac{1}{2\pi} \int_{-\infty}^{\infty} e^{i\omega t} \langle \rho(k,t)\rho(-k,0) \rangle dt, \qquad (23)$$

where

$$\rho(k,t) = \frac{1}{N} \sum_{i=1}^{N} \exp[-ikx_i(t)] \qquad (24)$$

is the Fourier transformed of the mass density in the chain (normalized to the particle number), and $\langle \cdot \rangle$ denotes an ensemble average. Generally, the SDF allows to estimate the time behavior of collective structures (excitations) formed by particles on specific length and time scales in a chain. By fixing the wave number k one can determine the corresponding frequency composition $S_k(\omega) = S(\omega,k)$. The width of a peak in the $S_k(\omega)$ spectrum gives an estimate the stability of the related excitation and of its velocity in the chain. For example, peaks with small width $\Delta\omega$ indicate high stability of the corresponding excitation.

Recently, the SDF was used to study nonlinear excitations in high-density rings [6]. In a ring the spectrum of wave numbers k takes discrete values k_i due to the periodic boundary conditions. More exactly, one finds

$$k_i = \frac{2\pi i}{L}, \qquad (25)$$

where $i = \pm 1, \pm 2, ..., \pm(N-1)/2$ for excitations traveling to the right $(+)$ or left $(-)$, respectively. In particular, $i = 0$ corresponds to slow rotations of the ring as a whole, and if $N = $ even then $i = N/2$ corresponds to optical anti-phase oscillations of neighbor particles. As will be demonstrated below, the SDF is an efficient tool for the analysis of excitations in low-density rings also.

All of our simulations for SDF calculations were carried out for rings with $N = 10$ particles. This has the advantage that the number of excitations is still rather small, allowing to observe in detail their transformation under parameter changes. Generally, all SDF plots will show normalized values 'SDF/SDFmax', where 'SDFmax' corresponds to the highest peak of the respective spectrum.

As a general rule, it is preferable to carry out time averages over many consecutive or partially overlapping time intervals $\Delta t \gg 1$ (in. $c.u.$) belonging to the same simulation run, instead of considering a large number of runs with different initial conditions. In particular, for the results presented in this paper we used simulation
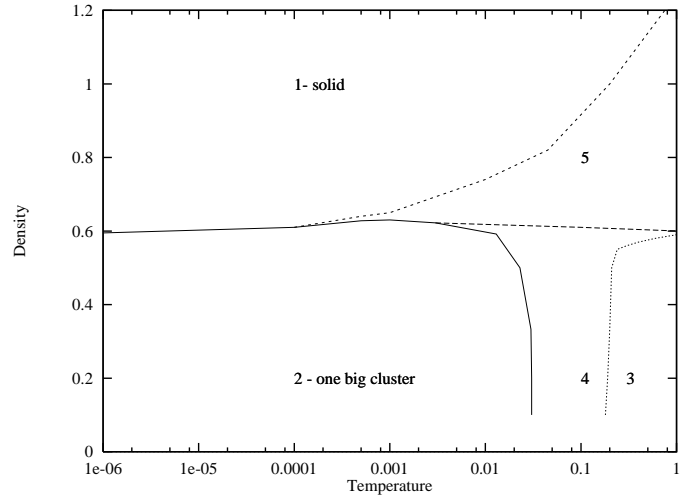
Fig. 3. Cluster phase diagram for the Morse ring with parameters $N = 4$, $b = 1$, $\mu = -\kappa, \gamma_0 = 1$ (no active friction). For this parameter setting the critical density value is given by $n_c = 0.59$. The lines symbolize transitions between different phase states: (1) solid-like lattice, (2) one big cluster (N-mer), (3) monomers prevail (gas-like), (4) small clusters (liquid-like), (5) strongly localized compressions (liquid-like). Note, that near the horizontal line, which indicates the critical density n_c, the other curves are not very reliable due to the especial geometrical definition used to characterize clusters. For example, for $n < n_c$ clustering states are destroyed if $T > \varepsilon$, where $\varepsilon = 0.5$ is the depth of Morse potential for $b = 1$.

runs of length $\Delta t = 4000$ (in $c.u.$), which were subdivided into 200 partially overlapping measurement intervals $\Delta_i t = 800\pi \gg 1$. This choice takes into account, that the frequency of oscillations is of order $\omega_0 = 1$ and, thus, the related period of oscillations $T = 2\pi$.

If the system has reached the stationary state, then it is sometimes also useful to switch off the heat bath during the SDF measurement by setting $\gamma_0 = 0$ and $D = 0$. This procedure allows to investigate the undisturbed dynamics of the collective excitations activated by the heat bath.

3 Results for the equilibrium system with $\gamma(v) \equiv \gamma_0$

3.1 Clustering phases in a finite-size Morse ring

In Figure 3 we plotted a 'phase diagram' constructed on the basis of numerically determined values for the cluster size probabilities $P_D[k]$ defined in Section 2.2. The diagram shows regions with different phase states for an ensemble with $N = 4$ particles in the temperature-density-plane. Although the particle number is very small, several different states can be observed. We also remark that Figure 3 essentially improves a rather rough schematic representation that was given in [17] and based on simulations with a less accurate Euler algorithm.

Low-density Morse ring ($n < n_c$)

Apparently, the corresponding region below the horizontal line in Figure 3 is divided in three parts by two curves indicating the transitions between different states. For very low temperature $T = D/\gamma_0$ the particles are primarily bound in one big cluster (region '2'), i.e., they constitute with high probability an N-mer. With increasing temperature T particles are more frequently split off the N-mer, leading to a change in the shape of the probability distribution $P_D[k]$. The temperature curve $T_{c1}(n)$, separating region '2' with $P_D[N] = 1$ from region '4' with $P_D[N] < 1$, may be considered as the first of several transition temperatures T_{cj} of the Morse chain. Even at very low densities the value $T_{c1}(n) \approx 0.03$ is noticeably less than the depth $\varepsilon = 0.5$ of the Morse potential with $b = 1$. A possible explanation might be that nonlinear collective excitations in the N-mer, similar to those in the high-density Toda-like chain, are responsible for its destruction at relatively low temperature values.

As already mentioned, with further increasing bath temperature T several k-mers may exist (region '4'), frequently splitting into smaller ones or recombining to bigger ones. Put differently, the system visits different metastable states corresponding to a mixture of clusters with different sizes – from the N-mer to monomers. Finally, there is a second critical temperature curve $T_{c2}(n)$ indicated by the dotted line, separating regions '4' and '3'. For $T > T_{c2}(n)$, in region '3', the cluster size distribution has only a single maximum $P_D[1]$, which is approximately equal to 0.2 at very low n and increases with $n \nearrow n_c$. Since the monomers have the highest probability here, this state may be classified as gas-like. Note, that due to our geometric cluster definition also $T_{c2}(n)$ is smaller than the depth ε of the potential (at least in the reliable region $n \not\approx n_c$). It was also checked that the simulations yield a positive energy $E > 0$ for $T > 0.5 = \varepsilon$, as it should be.

High-density Morse ring ($n > n_c$)

The high-density region $n > n_c$ in Figure 3 is divided in two parts. In the low-temperature region '1' clusters or compressions, respectively, do not exist. In contrast, such configurations sometimes arise in the high-temperature region '5'. This region can be interpreted as a liquid-like state, whereas the low-temperature region '1' is solid-like and phonon-dominated, respectively. Here distances between n.n. particles only slightly vary around $l = L/N$. Similar to before, we denote the critical temperature curve separating regions '5' and '1' by $T_{c3}(n)$. For $n = 1$ we find $T_{c3}(1) \approx 0.2$. If one takes into account, that

(i) the transition temperature T_{tr} for the specific heat of a Toda systems with our parameters is given by $T_{tr} = 0.1$ according to Bolterauer and Opper [26] and $T_{tr} = 0.16$ according to Ebeling and Jenssen [27], and

(ii) in Lennard-Jones systems T_{tr} approximately equals the depth ε of the potential well, then it is reasonable to assume that for Morse rings with $b = 1$ the inequality

$$0.1 < T_{tr} < 0.5 \tag{26}$$

holds, since they exhibit properties of both Toda and LJ systems. Thus, T_{c3} and T_{tr} can be considered as quantitatively closely related. Both quantities characterize the transition from solid-like to liquid-like states or phonons to cnoidal waves, respectively. This conclusion is also supported by the results presented of the subsequent sections.

3.2 Thermodynamic quantities

In this section we concentrate on the average force P, defined in equation (22) as a combined time and ensemble average. As already mentioned, we consider P as 'pressure', and, therefore, we are particularly interested in its behavior with respect to variations of temperature T and density n. Our numerical results, again for a ring with $N = 4$ particles, are represented in Figure 4a as isotherms P vs. l at $T =$ const., where

$$l := 1/n = L/N \tag{27}$$

is the specific volume, and in Figure 4b as isochors P vs. T at $l =$ const.

In Figure 4a one can observe anomalous behavior of the isotherms at small T near the critical density n_c. This effect is caused by the changing topological structure of the potential energy $U^M(x_1, \ldots, x_N)$ in this parameter region, i.e., by the appearance of new minima and maxima of U^M. In contrast to this, there is no anomalous behavior at high densities and low densities, since in both cases the thermodynamic properties are determined by phonons. More exactly, at low T and high density $n > \bar{n}_c$ the particles form an almost equidistant lattice on the ring, whereas at low T and small $n \ll n_c$ the N-mer is formed, which can be considered as a piece of solid with free ends and n.n. distances given by σ. Based on the properties of phonons we may deduce that $P \sim \omega(n)$, where for high-densities $\omega(n)$ is the linear oscillation frequency at the bottom of the effective potential, generated by the right and left neighbor of a particle. Furthermore, we can estimate that $P \sim \omega(1/\sigma) =$ const. at low densities. Upon considering the motion of the ith particle in the effective potential

$$U_i^{\text{eff}} = \frac{1}{2}(U_i^M + U_{i-1}^M), \tag{28}$$

it is not difficult to determine, that for high densities $n > \bar{n}_c$ and small oscillations at low T

$$\omega^2(n) = \omega_0^2 \left(2e^{\frac{-2b(1-n)}{n}} - e^{\frac{-b(1-n)}{n}} \right) \tag{29}$$

holds, where $\omega_0 = \sqrt{ab} = 1$ (in c.u.) as before. In particular, one obtains for $b = 1$, $\omega_0 = \omega(1/\sigma)$ and $n \approx 1$

$$P \sim \omega(n) \approx \sqrt{3n - 2} = \sqrt{3/l - 2}. \tag{30}$$

For $T < 0.1$ the two estimations for P are in good agreement with the numerically calculated isotherms in Figure 4a, as long as $n \not\approx n_c, \bar{n}_c$. In particular, the pressure in the N-mer approximately equals the pressure in a system

(a)

(b)
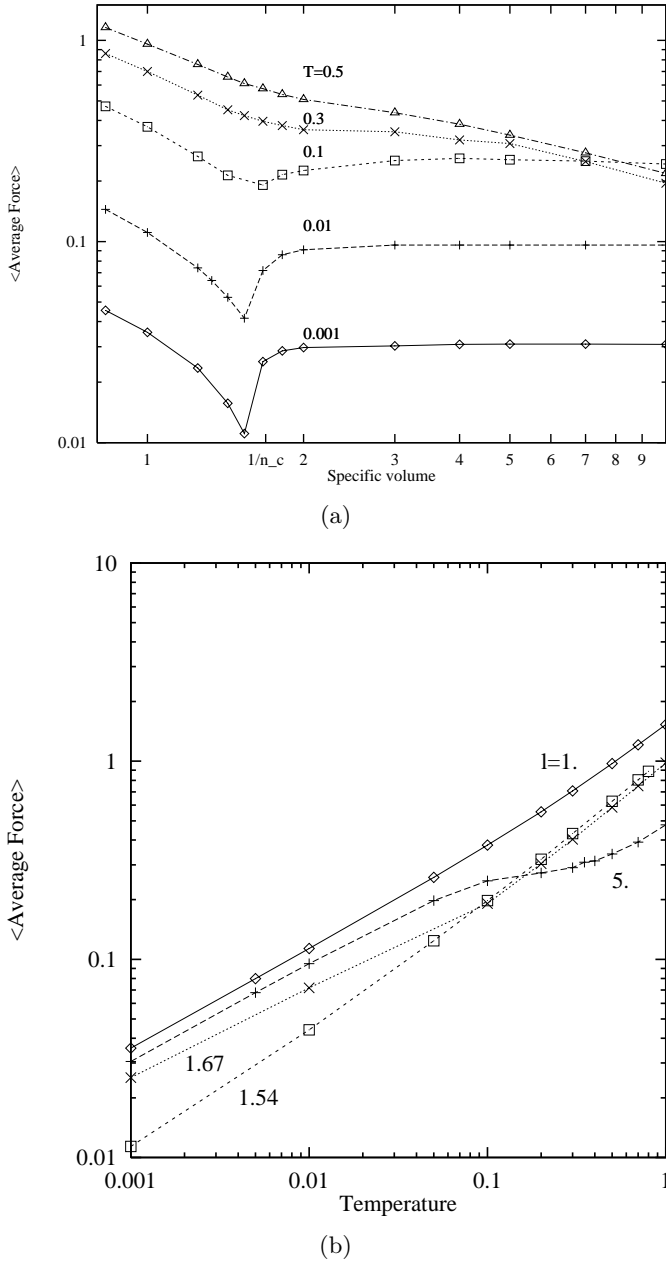
Fig. 4. Morse ring with $N = 4$ and $b = 1$. (a) Isotherms P *vs.* specific volume $l = 1/n$ at T =const. (b) Isochors P *vs.* T at l =const.

with density $n = 1$ and same temperature. For isotherms at $T > 0.2$ a region with power law behavior

$$P(l) \sim l^{-\alpha} , \qquad \alpha > 0, \qquad (31)$$

can be found for low density. Furthermore, with increasing temperature T the anomalous part of the isotherms disappears. For $0.5 < T \nearrow 1.0$, the numerical isotherms can, generally, in good approximation be described by the power law expression (31), but still with $\alpha < 1$. Thus, the system behaves rather liquid-like or real-gas-like than ideal-gas-like in this range. Another interesting effect

is the intersection of the 0.1-isotherm with the 0.3/0.5-isotherms at low density in Figure 4a. The system may have the same pressure P at different temperature values, because there can exist different phase states in the Morse ring.

In Figure 4b characteristic isochors P *vs.* T at constant specific volumes l are shown. The system with $l = 1$ corresponds to the the high density case, and, thus, its behavior is very similar to that of a Toda rings studied earlier [6]. Assuming that

$$P \sim T^{\beta} , \qquad \beta > 0, \qquad (32)$$

we find $\beta = 0.5$ at small temperature, as well-known from linear chain models. Then, for increasing temperature the characteristic exponent β also increases, that is, the Toda-like Morse lattice becomes more 'liquid'.

In the opposite case of very low density $n = 0.2 < n_c = 0.59$ corresponding to $l = 5$ a Morse ring behaves at small T like a solid or crystal, respectively. Its behavior changes dramatically near $T_{c2} = 0.2$, that is in the liquid-like region where $\beta \approx 0$. Then the isochor again rises with increasing β, approaching a gas-like state, though a pure gas state obeying a Clapeyron law with $\beta = 1$ is not yet reached at $T < 1$. In order to achieve ideal gas behavior the temperature must be increased further.

Finally, it is interesting to compare two Morse rings with slightly different densities near the critical value $n_c = 0.59$. The system with $l = 1.67$ ($n = 0.60$) behaves like a solid at small T, then transforms into a liquid-like state. In contrast, the ring with $l = 1.54$ ($n = 0.63$) behaves liquid-like both at small and high temperatures. In particular, its pressure P at low T differs essentially from that of the other three examples, which are rather solid-like at in the low temperature region. Consequently, in contrast to Toda systems, a Morse ring with n slightly higher than the critical density n_c may transform into a liquid-like state at low temperature due to the coexistence of qualitatively different stable configurations.

3.3 Microscopic properties: SDF spectra for a Morse ring with N = 10

Having so far only discussed macroscopic thermodynamic quantities, we now have a closer look at microscopic properties of Morse rings using the SDF $S(\omega, k)$.

All results presented in this part are based on computer simulations for rings with $N = 10$ particles and, as before, stiffness parameter $b = 1$. In particular, we are interested in the transformations of thermally excited excitations under variations of temperature and density. Generally, we concentrate on two types of excitations:

- excitations with spatial magnitude of a ring length L corresponding to the wave number $k = k_1$ where $k_1 = 2\pi/L$,
- excitations with spatial magnitude of an N-mer's length $L_{cl} = (N - 1)\sigma$ corresponding to $k = k_{cl}$ where $k_{cl} = \pi/L_{cl}$. This case is interesting if both temperature T and density n are low. Also note, that due
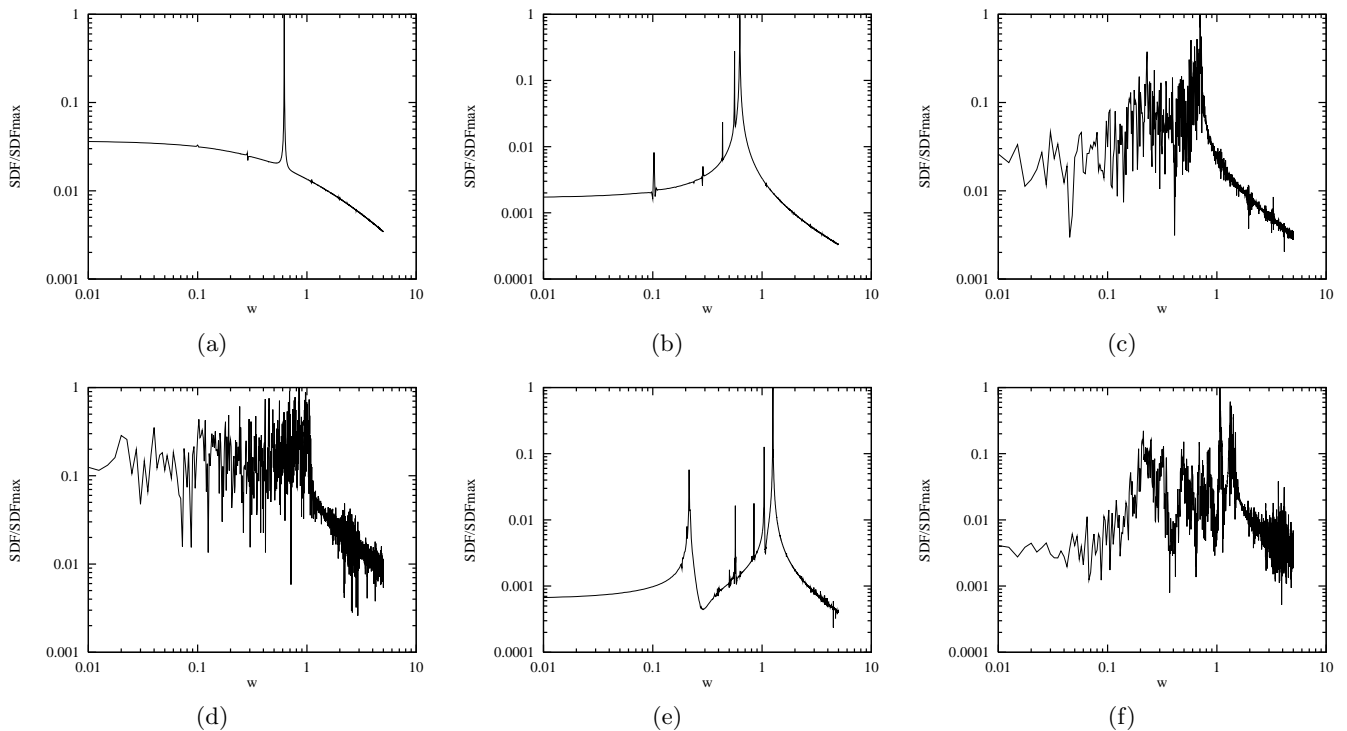
Fig. 5. High-density Morse chain with $N = 10$ and $b = 1$. Normalized dynamic structure factor SDF/SDFmax *vs.* ω for different temperatures values T and wave number $k_1 = 2\pi/L$. In (a-d) we have used density $n = 1$ and, thus, $k_1 = 0.628$. The last two pictures (e) and (f) are obtained for $n = 2$ and, thus, $k_1 = 1.257$. During the measurement of the spectrum the heat bath was switched off, $\gamma_0 = 0$ and $D = 0$. (a) For very low temperature $T = 0.0001$ one observes a phonon spectrum, similar to that of a linear chain. (b) For increased but still small temperature $T = 0.01$ nonlinearity effects lead to weak mixing of phonons. (c) In the region of the transition temperature, $T = 0.2 \approx T_{\text{tr}}$, the spectrum clearly changes. (d) For $T = 1.0 > T_{\text{tr}}$ the spectrum is very noisy. If the density is increased, as in Figures (e) and (f) where $n = 2$ was used, the Morse ring becomes more Toda-like. Then for $T = 0.2$, see Figure (e), the spectrum still looks very similar to (b) rather than (c). Moreover, for $T = 1.0$, as shown in (f), the first phonon begins to transform into a soliton-like structure, even though this excitation as well as the other phonons are less stable then in comparable Toda rings [21]. To summarize, compared with (c) and (d) the spectra in (e) and (f) are essentially less noisy, indicating that in a Morse chain collective excitations become more stable at high density.

to the different boundary conditions (open ends of the N-mer) there is no factor 2 in the wave number k_{cl}.

Before we discuss the results it might be useful to recall, when it is helpful to consider the SDF spectrum of a chain. The coupling of the chain to the heat bath is determined by the viscous friction coefficient γ_0 and the white noise amplitude D. Let us assume, that ω_0 is the characteristic frequency for the internal dynamics of the chain (dynamics without heat bath). Then one usually studies the SDF of the stationary state only if $\gamma_0 \ll \omega_0$ and $D \ll \omega_0 T$ holds. Otherwise, the noise perturbs the internal dynamics too strongly.

In contrast to macroscopic thermodynamic quantities like pressure, which should be merely connected to other thermodynamic quantities, *e.g.*, temperature or density, the SDF essentially depends on the microscopic parameters, as γ_0 or D in our case. More precisely, for different values of γ_0 or D realizing the same temperature value T, the SDF can be very different. As it turns out for our model, for $n \not\approx \bar{n}_c$ the SDF results only slightly depend on the above condition $\gamma_0 \ll \omega_0$, and we can neglect the influence of γ_0-variations in those cases. The situation is different for $n \in [n_c, \bar{n}_c]$. Here the evolution of collective

structures strongly depends on γ_0 and D, for they essentially determine the frequency of transitions between different potential minima and other metastable states. Due to this reason, we consider the SDF for different values of γ_0 and D, when dealing with the critical density region. In summary, we concentrate on the following three situations:

(i) high density $n = 1$ and $n = 2$, constant $\gamma_0 \ll 1$ and varying T;

(ii) low density, $n = 1/3$, constant $\gamma_0 \ll 1$ and varying T;

(iii) critical density $n \in (n_c, \bar{n}_c)$ and varying T for different constant values γ_0.

High-density Morse ring (Fig. 5)

We study the evolution of the SDF $S(\omega, k_1)$, where $k_1 = 2\pi/L$ corresponds to the resonance excitation in the ring with biggest spatial magnitude. At very small T this excitation is a phonon and its SDF spectrum, see Figure 5a for $n = 1/\sigma = 1$, is a single spectral line at $\omega = \omega_1$. Analogously, the spectra $S(\omega, k_i)$ with higher wave numbers

$k_i = 2\pi i/L$, $i = 2, 3, \ldots$ consist of a single spectral line at $\omega_i(k_i)$, corresponding to the ith phonon with frequency

$$\omega_i(k_i) = 2 \left| \omega_0 \, \sin\left(\frac{2\pi i}{L}\right) \right|. \tag{33}$$

For increasing but still small T the phonons begin to weakly interact with each other due to the nonlinearity of the potentials and, therefore, give birth to new peaks at small frequencies $\omega < \omega_1$, see Figure 5b. If the temperature is close to the transition temperature T_{tr} the structure of the spectrum changes essentially. The spatial structures are not very stable anymore. They interact and deform strongly, leading to many combined frequency components with $\omega < \omega_1$, see Figures 5c and d. This is different compared with Toda rings, in which at high temperatures relatively stable soliton-like excitations dominate the SDF spectrum. It can be supposed that this difference is due to the fact, that the topological properties of the Toda chain remain unchanged under variations of n, whereas in the Morse chain there may appear new local potential maxima/saddles if the distance between two n.n. particles becomes sufficiently large. Such topological changes may perturb nonlinear excitations and, thus, leads to a more continuous SDF spectrum, but nevertheless with prevailing components corresponding to nonlinear quasi-soliton-like structures. As pointed out several times before, with increasing density a Morse ring becomes more and more similar to a Toda ring. This is illustrated in Figures 5e and f, which were obtained for the same temperature values as in Figures 5c and d but higher density $n = 2$. Obviously, for an increased density value the excitations are more stable; the SDF spectrum becomes less noisy.

In Figure 6 we illustrated the fact that the SDF spectrum depends on the microscopic parameters γ_0 and D. One can readily see in this figure, how the spectrum essentially changes for $\gamma_0 \geq 0.1\omega_0$ and $D \geq 0.1\omega_0 T$. Intuitively, this can be explained by the now dominating influence of the heat bath, resulting in the destruction of collective particle dynamics. In this regime particles behave rather individually and the SDF spectrum is very noisy for a wide temperature range.

Low-density Morse ring (Fig. 7)

In case of $n < n_c$ the potential energy U^M has N equivalent minima, each corresponding to an N-mer configuration. For arbitrary initial conditions and small T, the influence of the surrounding bath causes the particles to choose one of the minima. Hence, the related excitations in the N-mer are phonons again. In particular, the internal dynamics is qualitatively similar to that of the chain with $n = 1$, even though the frequency composition of the SDF is different. The latter is now determined by the new boundary conditions, i.e., by the free ends of the N-mer. Therefore, the phonon of the biggest magnitude has a wave number $k_{cl} = \pi/(N-1)$, that is $k_{cl} \approx k_1/2$ for N large enough. For $n = 1/3$ the corresponding spectral line $\omega(k_{cl})$ can be clearly distinguished in Figure 7a. In fact,


(a)

(b)
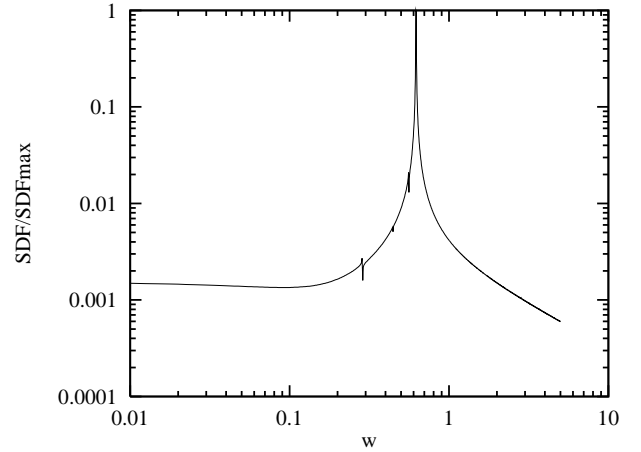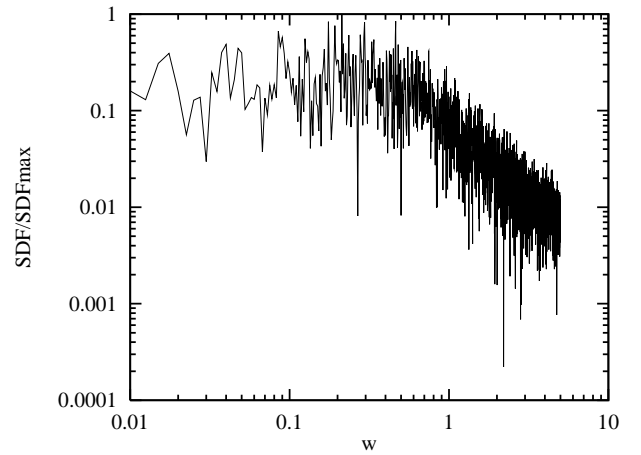
Fig. 6. γ_0-dependence of the SDF spectrum with $k_1 = 2\pi/L = 0.628$. Normalized dynamic structure factor SDF/SDFmax *vs.* ω for a Morse ring with $n = 1$, $N = 10$, $b = 1$ at very low temperature $T = 0.0001$. During the measurement for both pictures the heat bath was *not* switched off. (a) Weak friction $\gamma_0 = 0.001$ and (b) strong friction $\gamma_0 = 1.0$. One can clearly see, that for parameter values $\gamma_0 \geq \omega_0$ the SDF spectrum is of little value, if one wants to study collective excitations.

this picture also exhibits other lines at $\omega(ik_{cl})$ since the value $k = 0.628$, used for Figure 7a–d, is neither exactly equal to k_{cl} nor to $k_1 = 2\pi/L$. With increasing temperature the phonons are transformed into cnoidal waves, see Figure 7b; but when the cluster begins to break down at $T = 0.1 \approx T_{c1/2}$ a new effect is observed, see Figure 7c. Now the SDF spectrum looks like a $1/f$-spectrum, even if the heat bath is switched off during the stationary SDF measurement interval (i.e., $\gamma_0 = 0$ and $D = 0$). Put differently, the heat bath has excited a $1/f$-type internal dynamics. We suppose, that this is because the N-mer sometimes splits into two or three smaller clusters, which strike each other as big particles. In particular, a $1/f$-structure of the SDF spectrum is to be interpreted as an indicator for *phase transitions* in the chain, for it reflects

(a)

(b)

(c)

(d)
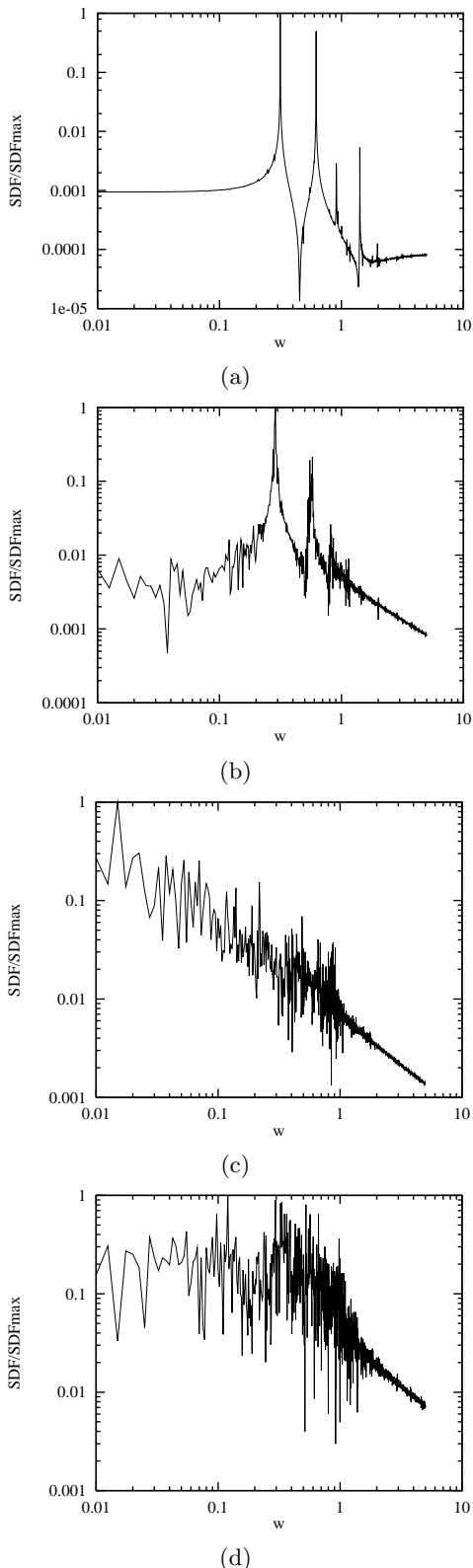
Fig. 7. Low-density Morse chain with $n = 1/3$ and $N = 10$, $b = 1$. Normalized dynamic structure factor SDF/SDFmax *vs.* ω for different temperatures and $k = 0.628$ in all pictures. During the measurement of the spectrum the heat bath was switched off, $\gamma_0 = 0$ and $D = 0$. (a) $T = 0.001$, (b) $T = 0.07$, (c) $T = 0.1$ and (d) $T = 0.5$.

the well-known fact that *near critical points correlations on all length and time scales become relevant.*

At higher (super-critical) temperatures $T \geq T_{c2}$ the clusters with smaller size and the monomers dominate, *i.e.*, the related cluster distribution function $P_D[k]$ exhibits only a single maximum at $k = 1$. The smaller k-mers create unstable excitations, similar to the high density case $n = 1$ discussed above. Consequently, the corresponding SDF spectrum looks similar to that of the high-density Morse ring. In particular this also means that beyond the critical temperature region the $1/f$-behavior is destroyed as shown in Figure 7d.

Morse ring in the critical density interval (Figs. 8–10)

All results presented in this part refer to the density value $n = 0.599$. According to equations (19, 20) and the facts summarized in Section 1.2, we find for the same value $b = 1$ as used before

$$n_c = 0.59, \qquad \bar{n}_c(10) > \bar{n}_c(3) = 0.61. \qquad (34)$$

Thus, $n = 0.599$ lies within the critical interval $[n_c, \bar{n}_c(10)]$, where both the equidistant distribution of the particles as well as the N-mers correspond to stable states, *i.e.*, they are minima of the full potential energy U^M. Hence, already at relatively low temperature values the system spontaneously switches from the state with uniform density to an N-mer configuration and *vice versa*.

According to our numerical results, for $n \in [n_c, \bar{n}_c(10)]$ there exist $1/f$-behavior of the SDF over a wide temperature range, see Figures 8, 9 and 10. However, the most interesting effects are observed at small temperatures. In Figure 8 one can see SDF spectra for very low temperature $T = 10^{-4}$ and different values of γ_0. Obviously, the SDF spectrum is essentially transformed, if γ_0 is changed. If the heat bath is switched off (*i.e.*, $\gamma_0 = 0$ and $D = 0$) during the SDF measurement (pure internal dynamics) one observes discrete peaks in Figure 8a corresponding to phonons. If γ_0 is increased while keeping $T = 10^{-4}$ constant, the SDF spectrum becomes more and more similar to a $1/f$-type spectrum, see Figures 8b and c. This fact indicates an increased destruction of regular collective excitations. During an intermediate stage, represented in Figure 8b, the SDF spectrum represents a mixture of the phonon spectrum and $1/f$-behavior. Which of the signals, phonons or $1/f$-noise, eventually dominate the SDF is mainly determined by the time that the system spends in the different metastable states. Compared with the phase diagram in Figure 3, we are dealing with the small transition area between regions '1' and '2' at low temperature, which also corresponds to the critical region in Figure 4a, where the isotherms show anomalous behavior. Most likely this state can be interpreted as a two-phase state. It is an interesting property of the Morse ring model, that such a state can exist at very low temperatures, and, in particular, in a narrow density interval between regions corresponding to two rather solid-like states (lattice for $n > \bar{n}_c$ and N-mer state for $n < n_c$).

(a)

(b)

(c)
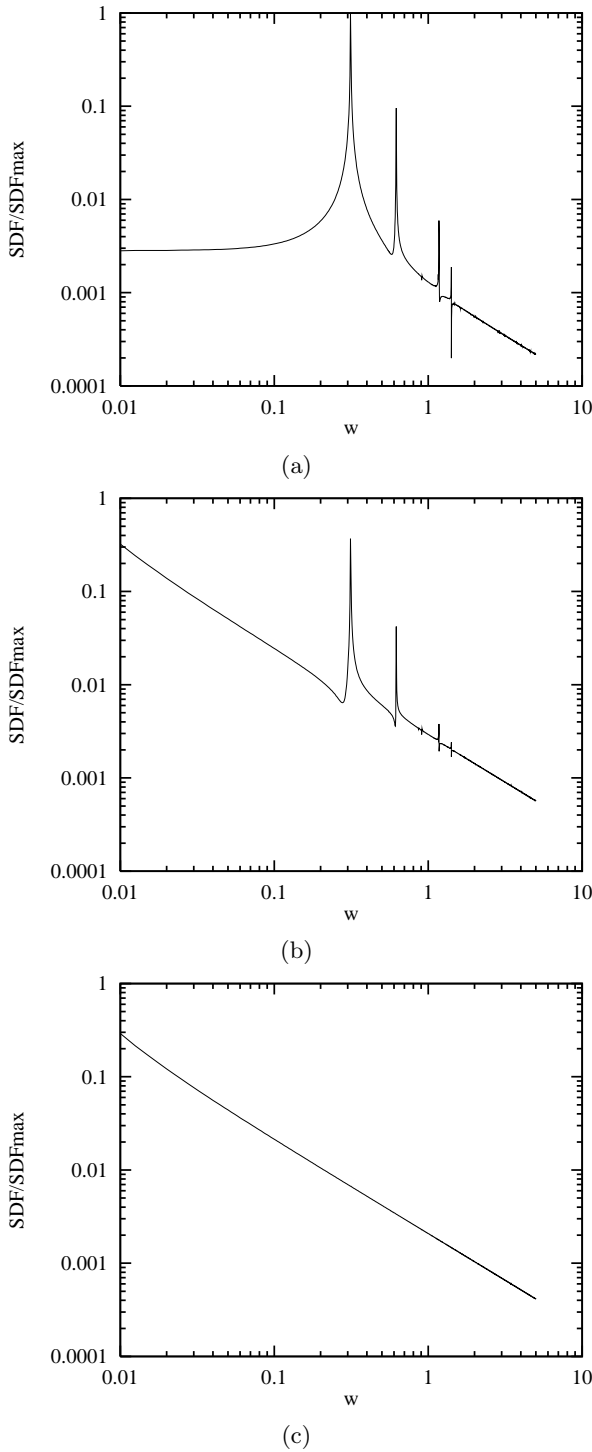
Fig. 8. Morse ring with density $n = 0.599 \in (n_c, \bar{n}_c)$ and parameters $N = 10$, $b = 1$. SDF/SDFmax *vs.* ω for $k_1 = 2\pi n/N = 0.376$, very low temperature $T = 10^{-4}$ and different values γ_0. In (a) the heat bath was switched of during the measurement, *i.e.*, $\gamma_0 = 0$ and $D = 0$, whereas in (b) $\gamma_0 = 10^{-8}$ and in (c) $\gamma_0 = 10^{-5}$. Note, that in (b) and (c) the values corresponding to SDFmax cannot be seen, since they are located in the region $\omega < 0.01$, which is not shown here. As one can readily see in (b) and (c), the presence of the heat bath during the measurement induces a $1/f$-behavior in the formerly phonon-dominated spectrum.

(a)

(b)
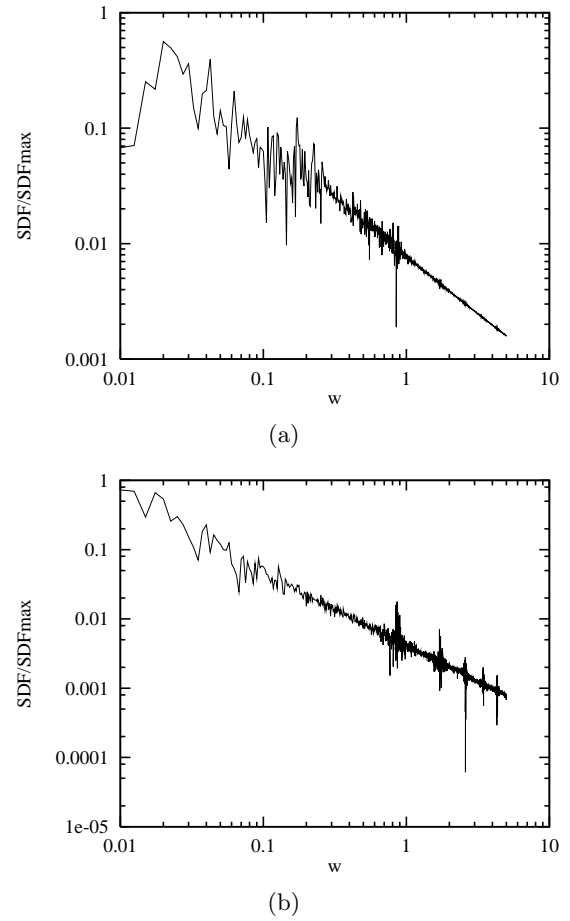
Fig. 9. Morse ring with density $n = 0.599 \in (n_c, \bar{n}_c)$, $N = 10$ and $b = 1$. Normalized dynamic structure factor SDF/SDFmax *vs.* ω at moderate temperature $T = 0.1$ for $k = 0.376$. During the measurement of (a) the heat bath was switched off $\gamma_0 = 0$ and $D = 0$. During the measurement of (b) the heat bath was present with $\gamma_0 = 1$. In both diagrams the values corresponding to SDFmax cannot be seen, since they are located in the region $\omega < 0.01$. In contrast to the low temperature case shown in Figure 8, there now also exists $1/f$-behavior if the heat bath is switched off during the measurement, compare Figure 8a and Figure 9a.

For higher temperature $T = 0.1$ there is again $1/f$-behavior as shown in Figure 9. The difference to before is that this behavior is now also observable, when the heat bath is switched off during the measurement as the case in Figure 9a. That means that *at this temperature the internal dynamics is characterized by $1/f$*, as it was also observed for low density $n = 1/3 < n_c$ in Figure 7c. Moreover, for $T = 0.1$ the coupling to the heat bath during the SDF measurement merely enhances the internal $1/f$-behavior, see Figure 9b. In principle this is similar to Figure 8c.

Finally, in Figure 10 we also plotted the SDF for relatively high temperature $T = 0.5$. This value exactly corresponds to the depth of the Morse potential with $b = 1$. Generally, at high temperature the peculiarities in the spectra disappear due to the now dominating influence of the bath. At small γ_0-values, see Figure 10a and b, the

(a)

(b)

(c)
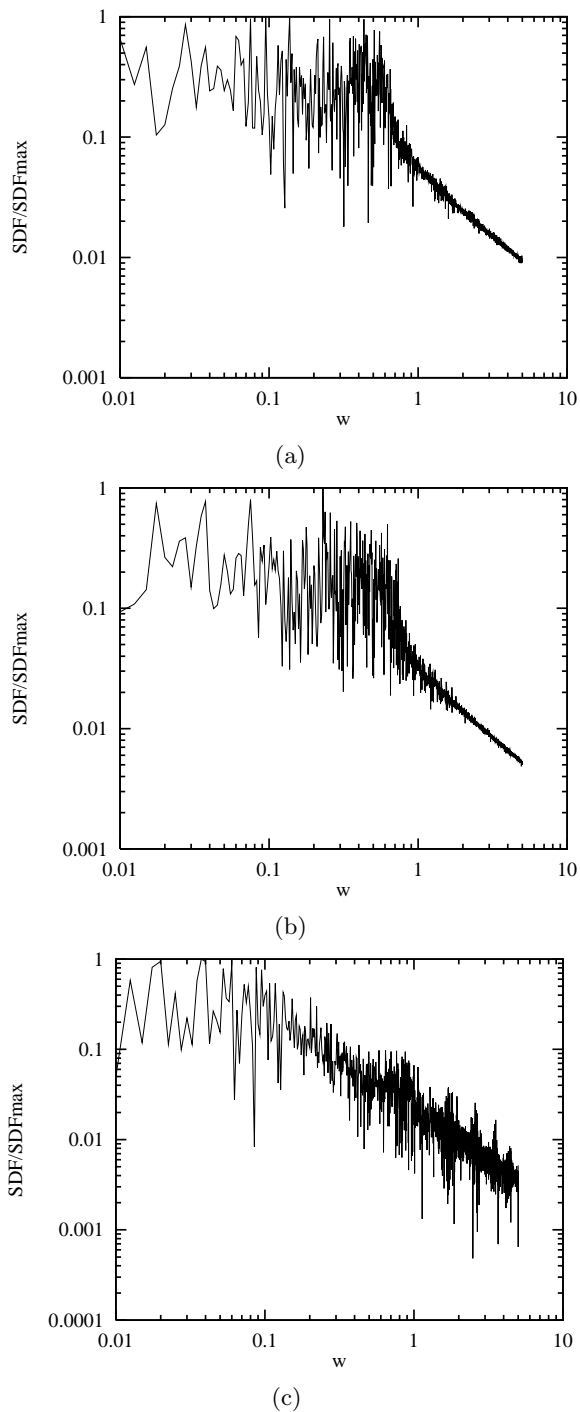
Fig. 10. Morse ring with density $n = 0.599 \in (n_c, \bar{n}_c)$, $N = 10$ and $b = 1$ at high temperature $T = 0.5$ and different values γ_0 during the measurement. Normalized dynamic structure factor SDF/SDFmax *vs.* ω for $k = 0.376$ and (a) $\gamma_0 = 0$, (b) $\gamma_0 = 0.001$, (c) $\gamma_0 = 1$.

SDF spectrum looks more or less similar to those obtained for $n = 1$ and $n = 1/3$, compare Figure 5d and 7d. On the other hand, at large γ_0-values, see Figure 10c, the related SDF is not very different from the spectrum at, for example, $n = 1$ and $\gamma_0 = 1$, that was shown in Figure 6b.
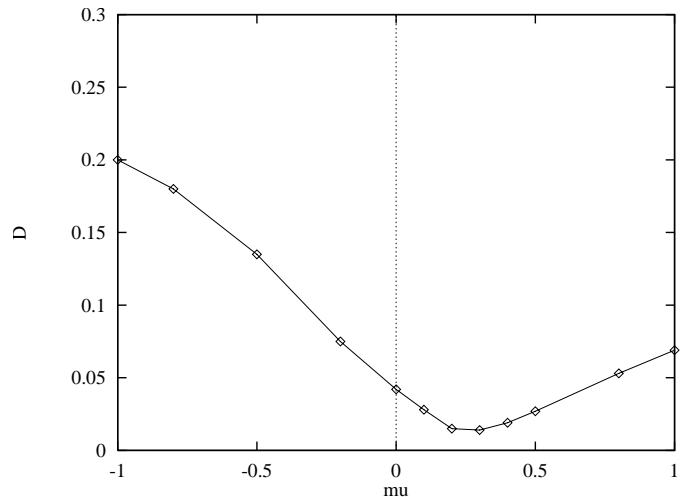
Fig. 11. Active Morse ring with parameters $N = 4$, $\gamma_0 = 1$, $n = 1/3$, $\kappa = 1$. Critical noise amplitude D_{c2} as function of μ. As before all quantities are given in *c.u.*

4 A far-from-equilibrium effect

Until now we exclusively discussed results for the equilibrium system with purely viscous friction, *i.e.*, $\gamma_1(v) \equiv 0$. In the remainder we turn our attention to the non-equilibrium case characterized by a nonlinear contribution $\gamma_1(v) \neq 0$ to the effective friction coefficient $\gamma(v) = \gamma_0 + \gamma_1(v)$, as given in equation (16). The deterministic limit case, corresponding to temperature $T = 0$ of the heat bath, has already been extensively studied for active Toda ring chains [10,28], as well as for active Morse rings [17]. The main results of these to a large extent analytical studies can be summarized as follows: Generally, for active systems one can find stable stationary states (attractors), either corresponding to rotational or oscillating modes (nonlinear waves). The stationary energy of such stable motions is primarily determined by the parameters of the combined friction coefficient $\gamma(v) = \gamma_0 + \gamma_1(v)$. Moreover, the stationary modes always look very similar to sinusoidal phonon excitations at small energies or cnoidal soliton-like waves at high energies, known from the related conservative system. In particular this means that in active Toda rings stable running soliton excitations may be generated [8,10,28]. In [10] this was even experimentally confirmed for Rayleigh friction.

In the remainder of this paper, we focus on the properties of an active Morse system at low density. In particular, we would like to know how the fragmentation of the N-mer into smaller k-mers depends on the parameter μ, which encodes the uptake of energy from an external reservoir and its conversion into kinetic energy of motion. To this end, we determine the critical noise amplitude $D_{c1} = T_{c1}\gamma_0$, at which destruction of the N-mer begins, as a function of the parameter μ. As before in Section 3.1, the probability distribution $P_D[k]$ will be used for the identification of this transition.

In Figure 11 one can see the results for an active Morse ring with parameters $N = 4$, $\gamma_0 = 1$, $\kappa = 1$ and $n = 1/3$.

The diagram shows, how the value D_{c1} behaves, when the parameter μ is increased from the equilibrium value $\mu_{eq} = -\kappa$ to values $\mu > 0$ corresponding to over-critical pumping.

Interestingly, the curve D_{c1} *vs.* μ exhibits a minimum at $\mu_c \approx 0.25$. This means that there exists a minimal value $D_{c1min} \approx 0.025$, such that the big cluster is never destroyed by increasing μ, as long as $D_{c1} < D_{c1min}$. Alternatively one can say that for $\mu > \mu_c$ pumping stabilizes the cluster compared with the case $D_{c1} = D_{c1min}$.

An explanation for this unusual effect might be, that for $\mu > \mu_c$ the deterministic energy, pumped into the particles by virtue of $\gamma_1(v)$, is primarily converted into 'well-directed' kinetic energy of motion. For large enough value of μ the dissipative force connected with $\gamma_1(v)$ dominates over the noise and, in particular, stabilizes rotating cluster on the ring (the particles feel an effective temperature, which is lower than the actual temperature of the heat bath). Such cluster stabilizing effects of nonlinear friction should be subject of more detailed investigations in the future.

5 Summary and conclusions

In this work we discussed numerical results for a $1d$-model of N Brownian particles with periodic boundary conditions ($N \leq 10$). We considered n.n. Morse interactions, which are repulsive at short distances and attracting at intermediate and long distances. Using this type of interaction our model converges to the well-known Toda model at high densities, whereas at low densities clustering effects dominate (similar to Lennard-Jones chains).

A Morse ring can be characterized by two different critical density values n_c and $\bar{n}_c$, where $n_c = \bar{n}_c$ for $N = 2$ and $n_c < \bar{n}_c$ for $N > 3$. For $n > n_c$ the equidistant configuration is a minimum of the full potential energy U^M, and for $n < \bar{n}_c$ there exist N equivalent minima of U^M corresponding to clustering states (N-mers). In the critical interval $(n_c, \bar{n}_c)$ both types of minima coexist. This leads to interesting effects, when the ring is coupled to a heat bath.

The stochastic Langevin equations of motion (e.o.m.) were numerically integrated using an adapted 4th order Runge-Kutta method. On the basis of the numerical solutions, phase diagrams for different density and temperature values were calculated. By analyzing the diagrams for a finite-size Morse ring ($N = 4$), five different thermodynamic states can be classified. Simple analytic estimates for the related pressure support the numerical results. Moreover, we also investigated collective excitations in a Morse ring with $N = 10$ particles by means of the spectrum of the dynamical structure factor (SDF).

In particular, one is able to distinguish two different types of liquid-like states of the Morse chain. The first one is observed at subcritical density values $n < n_c$ and moderate temperature of the heat bath. It can be characterized as mixture of meta-stable k-mers (smaller clusters of bound particles). The second liquid-like state can be observed at intermediate-to-high temperatures and supercritical densities, $n > n_c$. This state is very similar to the high-temperature state of the Toda chain, which is characterized by thermally excited cnoidal waves.

The transition regions between different phase states are related to changes in the SDF spectrum, where several types of $1/f$-behavior can be observed. In principle, this reflects the well-known fact that *near critical points correlations on all length and time scales are important.* Since the SDF can be measured in inelastic scattering experiments, it can be a useful tool in order to investigate phase transitions in real systems.

In the last part, we still presented a numerical result for an active chain, which is realized by an additional non-linear dissipative force term in the equations of motions. By virtue of this force, which can lead to negative friction due to external non-thermal pumping, the system may be driven to far-from-equilibrium states. The numerical results indicate that such an additional energy exchange mechanism can stabilize cluster configurations.

References

1. E. Fermi, J. Pasta, S. Ulam, In *Collected Papers of Enrico Fermi II* (University of Chicago Press, Chicago, 1965), p. 978
2. *Physics in One Dimension*, edited by J. Bernasconi, T. Schneider (Springer Verlag, 1981)
3. M. Toda, in *Nonlinear Waves and Solitons* (Kluwer Acad. Publ., Dordrecht, 1983)
4. M. Toda, N. Saitoh, J. Phys. Soc. Jpn **52**, 3703 (1983)
5. S.E. Trullinger, V.E. Zakharov, V.L. Pokrovsky, edited by *Solitons* (North Holland, Amsterdam, 1986)
6. W. Ebeling, A. Chetverikov, M. Jenssen, Ukrain. J. Phys. **45**, 479 (2000)
7. M. Jenssen, W. Ebeling, Physica D **141**, 117 (2000)
8. W. Ebeling, U. Erdmann, J. Dunkel, M. Jenssen, J. Stat. Phys. **101**, 443 (2000)
9. C.I. Christov, M.G. Velarde, Physica D **86**, 323 (1995)
10. V. Makarov, W. Ebeling, M. Velarde, Int. J. Bifurc. Chaos **10**, 1075 (2000)
11. V.A. Makarov, E. del Rio, W. Ebeling, M.G. Velarde, Phys. Rev. E **64**, 036601 (2001)
12. M. Schienbein, H. Gruler, Bull. Math. Biology **55**, 585 (1993)
13. A.S. Mikhailov, D. Zanette, Phys. Rev. E **60**, 4571 (1999)
14. W. Ebeling, F. Schweitzer, B. Tilch, BioSystems **49**, 17 (1999)

15. P. Morse, Phys. Rev. **34**, 57 (1929)
16. J. Dunkel, W. Ebeling, U. Erdmann, Eur. Phys. J. B **24**, 511 (2001)
17. J. Dunkel, W. Ebeling, U. Erdmann, V.A. Makarov, Int. J. Bif. & Chaos **12**, 2359 (2002)
18. J. Dunkel, W. Ebeling, J.W.P. Schmelzer, G. Röpke, in *Nucleation Theory and Applications*, Chap. 16, *Dissipative Collisions of One-Dimensional Morse-Clusters with Intermediate Energy Storage* (JINR Publishing House Dubna, 2002). ISBN 5-9530-0005-7, 367pp.
19. W. Ebeling, J. Ortner, Physica Scripta T **84**, 69 (2000)
20. W. Ebeling, A. Chetverikov, *Complex dynamics and nonlinear excitations in rings of interacting Brownian particles* in *Attractors, Signals, and Synergetics*, Vol. 1 (Pabst Science Publishers, Lengerich, 2002), p. 25
21. A. Chetverikov, W. Ebeling, M. Jenssen, Yu. Romanovsky, *Excitations on rings of molecules* in *Stochastic Dynamics of Reacting Biomolecules*, Chap. 5 (World Scientific, 2003)
22. F. Schweitzer, W. Ebeling, B. Tilch, Phys. Rev. Lett. **80**, 5044 (1998)
23. U. Erdmann, W. Ebeling, L. Schimansky-Geier, F. Schweitzer, Eur. Phys. J. B **15**, 105 (2000)
24. Yu. L. Klimontovich, Physics-Uspekhi **37**, 737 (1994)
25. N.N. Nikitin, V.D. Razevich, J. Comput. Math. Math. Phys. **18**, 108 (1978) (in Russian)
26. H. Bolterauer, M. Opper, Z. Phys. B **42**, 155 (1981)
27. W. Ebeling, M. Jenssen, SPIE **3726**, 112 (1999)
28. W. Ebeling, P.S. Landa, V. Ushakov, Phys. Rev. E **63**, 046601 (2001)